

Characterization of Visible Range Gain in Praseodymium Doped Fiber Amplifier

Nasrin Sultana¹, Md. Abubakar Siddik²

^{1,2}Department of Electronics and Communication Technology, Hajee Mohammad Danesh Science and Technology University, Dinajpur-5200, Bangladesh

Corresponding author: Nasrin Sultana

DOI: <https://doi.org/10.52403/ijrr.20240115>

ABSTRACT

In the optical (380-700 nm) region, a simulation study was conducted to assess the low-signal gain, power conversion efficiency (PCE), and optical output power of a praseodymium-doped fiber optic amplifier (PDFA). The PDFA performance was assessed using the optimized Pr³⁺ fiber length, Pr³⁺ ion concentration, and pump power. Additionally, the effects of input signal voltage and amplifier gain on amplified spontaneous emission (ASE) were investigated. A lower peak signal of roughly 1 dB at 635 nm was obtained with a shorter 5 m Pr³⁺ doped fiber and a higher pump power of 300 mW. The impact of wavelength and pump power variations on the amplifier's optical output power's spontaneous enhanced emission (EEM) is examined. Finally, the ionic interaction (general-purpose conversion effect) in the low-power amplifier signal is analyzed by taking into account various values of the upconversion factor.

Keywords: Praseodymium doped fibre amplifier, Small-signal gain, Pump power, Ultrashort laser.

INTRODUCTION

Ultrafast optics has long been a popular area of research. Over the past ten years, ultrafast-mode fiber lasers have found applications in industrial and medical settings, as well as optical imaging and micromachining [1,2]. Furthermore, it is widely used in the domains of supercontinuum spectrum generation, terahertz generation, and fiber frequency tuning [3-6]. With its short pulse width and high energy, distributed soliton (DS) lasers are among the most attractive types of fiber lasers. DS lasers are capable of producing single-mode beams with up to 31 nJ of power per oscillator, the highest femtosecond pulse energies yet achieved by standard beam lasers [7].

Fiber amplifiers are a promising device for the direct amplification of optical signals in fiber optic transmission systems. Chun Jiang and Li Jin created a theoretical model in 2009 to explain the gain variation along the fiber's length [8]. AV Smith et al. [9] provided a numerical demonstration of the population inversion saturation and stimulated thermal Rayleigh amplification associated with laser amplification of a large-mode fiber amplifier. Chen Peiyong et al. (2012) [10] suggested a numerical Euler method solution to the fiber optimizer's frequency equation's initial value problem. Because of the unique properties and possible advantages of active fibers, heavily doped phosphate fibers were used [11].

In the past few years, a great deal of research has been conducted on doped Fiber amplifiers using rare earth metal dopants like praseodymium, erbium, thulium, and ytterbium [12–18]. A small doping radius is advised for the erbium-doped fiber amplifier (EDFA) in order to maximize gain and accomplish effective pumping [19]. Er³⁺, Yb³⁺, and Pr³⁺-based synthetic

fiber enhancers have been proposed in [20, 21]. The measurement of the amplification efficiency was done at infrared region. The proposed advanced composite fiber amplifier produced a 38 dB raw power variation and less than 3 dB gain variation between 1.53 and 1.565 μm [22]. Aluminum, erbium, zirconium, and yttrium were among the gain media. The thulium-doped fiber amplifier (TDFA) shows a signal gain of approximately 41 dB, 45 dB, and 30 dB at 1.9 μm , 1.95 μm , and 2 μm , respectively. A variety of effective PDFFA models operating at approximately 1.3 μm are available in References [23, 24]. By varying the Judd-Ofelt parameters, the effect of the stimulated emission cross-section can be enhanced by taking into account the effects of temperature on Pr^{3+} ion concentration, ASE interference, and device fabrication components. With an energy conversion efficiency of at least 4.5 μm , the Pr^{3+} ion-doped broadband mid-infrared chalcogenide fiber amplifier boasts a high gain of 25 dB and 62.8 dB in the 4-5 μm range. 4.3-5.3 μm , in that order [25, 26].

As the previous discussion showed, none of the papers deal with ultrafast lasers with visible range. This work evaluates the performance of the PDFFA in the visible range through a comprehensive simulation-based analysis using OptiSystem, a commercial software tool from Optiwave Corporation [27]. Pr^{3+} doped at the optimal dopant concentration was used to create a high-efficiency optical amplifier model that maximized both the pump power and the fiber length. Therefore, it is thought that by using the suggested PDFFA design, developers can maximize the performance of the finished product.

MATERIALS & METHODS

The development of doped fiber amplifiers, which can boost signals in the optical domain and supply several optical wavelengths with a high gain. Doped fiber amplifiers can be made with rare-earth dopants, primarily erbium, thulium, praseodymium, and ytterbium [28]. Figure 1 shows the emission spectra of several rare-earth doped fibers.

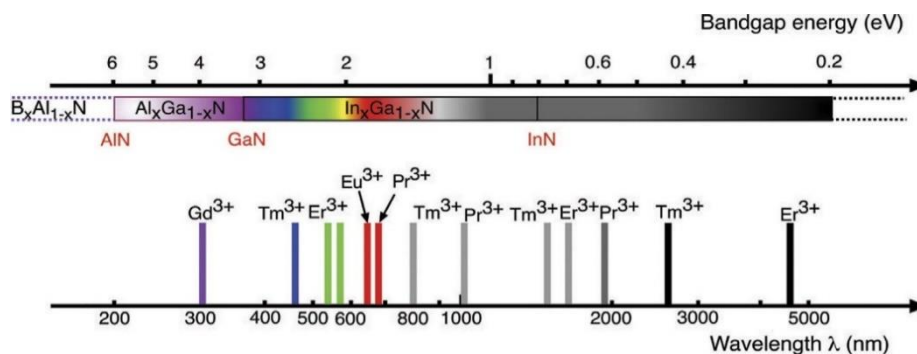


Figure 1. Emission spectra from rare-earth doped fiber

High conversion rates and visible output are offered by fiber-based lasers, using internal frequency shift are gaining popularity. An optical fiber with a large surface area that enables efficient cooling serves as the active medium. Because of its optical characteristics, an optical fiber's transverse mode quality is significant. Because of their red emission, fiber lasers can replace low-energy, high-energy ion or metal vapor lasers in a variety of other applications, such as biological and medical ones. Blue and green have constrained bandwidths. As a result, research focuses on employing diode laser pumps to boost emission in various spectral lines and enhance overall performance.

When a medium absorbs two infrared (IR) photons and responds by releasing one visible photon, this phenomenon is known as lasing by up conversion. Physically, stepwise excitation

through an intermediate level populates a highly excited energy level. When a level transitions from an intermediate level to the ground state, lasing may happen. One pump source is needed if the intermediate level's energy is half that of the highly excited level.

The nearly ideal energy-level scheme of the praseodymium ion (Pr^{3+}) allows it to cross the intermediate $1G_4$ level at 850 nm and travel two photons to reach the highly excited level (Fig. 2). Conversely, the maximum cross section of the ground state to $1G_4$ transition is approximately 1035 nm. This excitation is inefficient because it only occurs by a "wing" transition when pumped at 850 nm (step 1). Between 840 and 860 nm is the optimal wavelength for the second transition (step 2) from $1G_4$ to $3P_0$. This mismatch in excitation wavelengths can be fixed in one of two ways: either employ a second pump wavelength of 630 nm, or convert 850 nm pump photons using the proper co-dopant.

This makes use of Yb^{3+} . Step 3 absorbs four total IR photons, which effectively populates its $2F_{5/2}$ level in a nonradiating process. Step 4 involves resonant energy transfer to an alternative Pr^{3+} ion. As a result, two extremely excited Pr^{3+} ions are prepared for laser production. This pumping scheme is called an avalanche process because three more photons are absorbed more efficiently after the first photon is absorbed less efficiently. After pumping to the lowest sublevel and completing radiation-free decay, the highly excited $3P_0$ of Pr^{3+} is finally ready to emit a competing transition to the level of the ground multiplet to be used as a lasing transition.

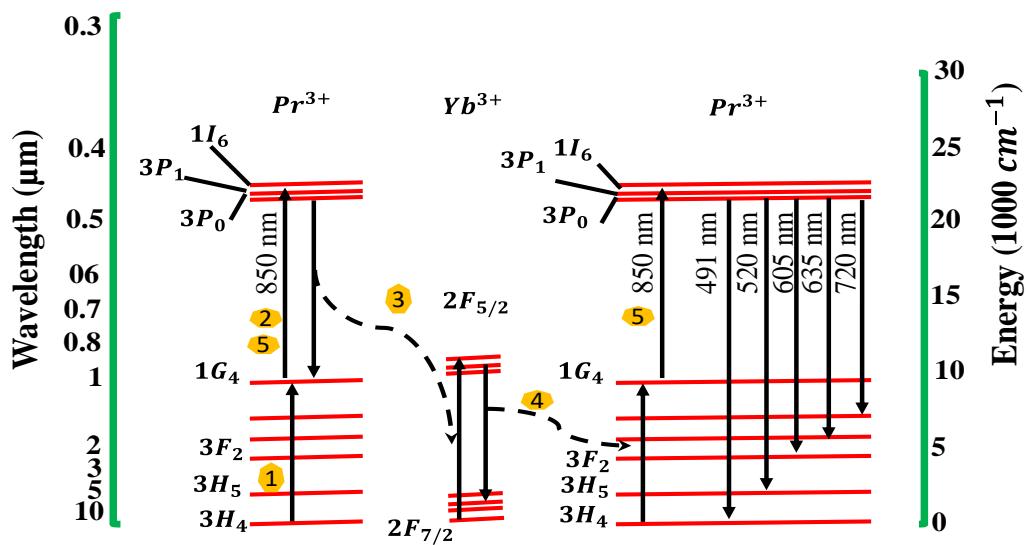


Figure 2: Upconversion process of praseodymium ion

The numbers $1G_4$, $3P_0$, $3P_1$, $1I_6$, $3F_2$, $3H_5$, and $3H_4$ represent the primary energy level transitions. The GSA pump and emission are made possible by the transition from $1G_4$ to $3H_4$. Similarly, the transitions $1G_4 \rightarrow 3H_5$ and $3H_4 \rightarrow 3F_4$ hold signal emission and ground state absorption (GSA). Furthermore, since the energy variance concerning the $1G_4$ and $1I_6$ levels equals the energy variance concerning the $1G_4$ and $3H_5$ levels, the up-conversion effect caused by the $1G_4 \rightarrow 1I_6$ and $1G_4 \rightarrow 3H_5$ transitions can lower the carrier concentration of the $1G_4$ level [29]. The overall density, n_t , is determined by the carrier concentrations at each level, signified by the numbers n_1 , n_2 , n_3 , n_4 , and n_5 .

$$n_t = n_1 + n_2 + n_3 + n_4 + n_5 \tag{1}$$

The rate equations for the Pr³⁺ energy level diagram in Fig. 2 can be expressed as follows:

$$\frac{dn_3}{dt} = \gamma_{13}n_1 - \left(\gamma_{35} + \gamma_{34} + \gamma_{32} + \gamma_{31} + \frac{1}{\tau_3} + cn_3\right)n_3 + \frac{B_{43}}{\tau_4}n_4 + \frac{B_{53}}{\tau_5} \quad (2)$$

$$\frac{dn_4}{dt} = \left(\gamma_{35} + \frac{c}{2}n_3\right)n_3 - \frac{n_4}{\tau_4} \quad (3)$$

$$\frac{dn_5}{dt} = \gamma_{35}n_3 - \frac{n_5}{\tau_5} \quad (4)$$

In Eq. (2) to (4), the transition rates γ_{13} , γ_{31} , γ_{31} , γ_{34} , and γ_{35} are given by $\frac{P_p\sigma_{13}np}{A_c h\nu_p}$, $\frac{P_p\sigma_{31}np}{A_c h\nu_p}$, $\frac{P_p\sigma_{32}np}{A_c h\nu_p}$, $\frac{P_p\sigma_{34}np}{A_c h\nu_p}$ and $\frac{P_p\sigma_{35}np}{A_c h\nu_p}$, respectively. Similarly, B_{53} and B_{43} are branching ratios for the $^3P_0 \rightarrow ^1G_4$ and $^1I_6 \rightarrow ^1G_4$ transitions.

The transitions between the 3H_4 and 1G_4 levels, which have carrier densities of n_1 and n_3 , respectively, dictate the PDFA's full small-signal gain. The signal propagation equation can be expressed as follows [29] when the PDFA with a depth of dz travels using PDFA as a gain medium:

$$\frac{dP_s}{dz} = [n_3(\sigma_{32} - \sigma_{34}) - n_1\sigma_{13}]P_s\Gamma_s \quad (5)$$

The excited state absorption (ESA) cross-section at the signal wavelength (σ_{34}) is not taken into account by OptiSystem in the given expression. Thus, the obtained signal efficiency is given by [29].

$$G = \frac{P_s(L)}{P_s(0)} = \exp [L\Gamma_s \{n_3(\sigma_{32} - \sigma_{34}) - n_1\sigma_{13}\}] \quad (6)$$

where PDF length is L.

SIMULATION SETUP

The proposed PDFA implementation plan is illustrated in Fig. 3. Two optical isolators, a WDM coupler, a laser pump source, and a brief fiber section with Pr³⁺ ions make up the amplifier. Optical isolation is employed in this configuration to minimize performance-degrading back emissions, stabilize amplifier operation, and stop the amplifier from operating as a laser. A laser with a wavelength of $p = 6.3 \mu\text{m}$ and a pump power of 300 mW as the gain medium PDFA. Short wavelengths are used in indirect pumping to activate the Pr³⁺ ions in the PDFA growth medium. Usually, the ground area (GSA) is injected using short wavelengths up to 1.03 μm . A brief wavelength of 840 can be employed for indirect excitation.

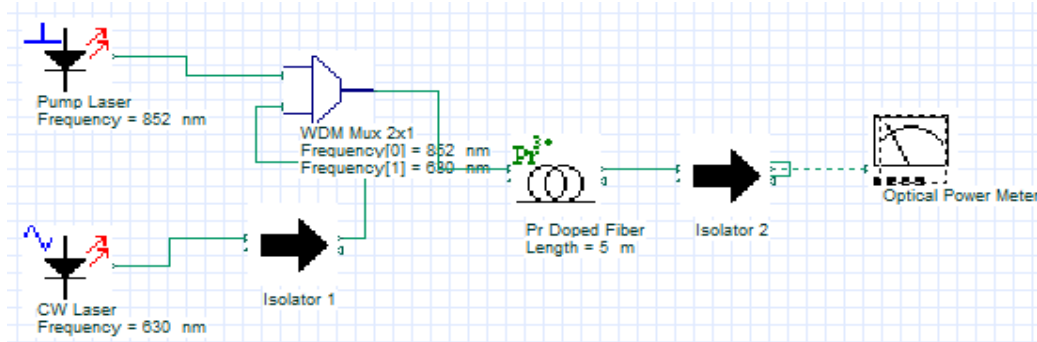


Figure 3.: Schematic of the proposed setup for PDFA

RESULTS & DISCUSSION

Figure 4 considers the optimized MFD, Pr³⁺ concentration, and PDF length for a signal power of -65 dBm. The signal wavelength is plotted against the pump power and the ASE noise power.

Using a signal wavelength of 850 nm and a pump power of 300 mW, it can be seen that the highest ASE is near -45 dBm. Due to spontaneous emission, more photons are produced during optical amplification as the pump power increases. As a result, the sound power of ASE increases with pump power. Furthermore, at longer wavelengths, the ASE exhibits a significant decreasing trend, which could be explained by the absence of population inversion at these longer wavelengths.

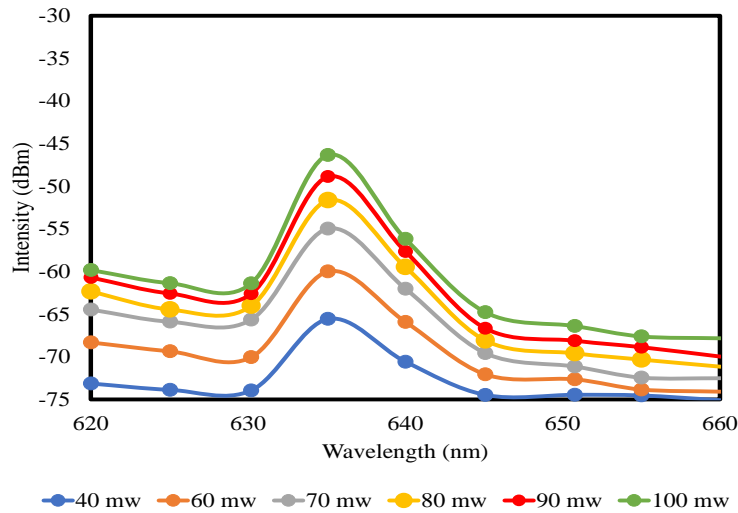


Figure 4: Signal wavelength plotted against ASE as a function of pump power

The up-conversion effect, an ion-ion interaction that impacts PDFA performance, is connected to Pr³⁺ concentration in PDF. Up-conversion usually has a negative effect on PDFA performance when PDF has a high Pr³⁺ concentration ($n_t > 50 \times 10^{24} \text{ m}^{-3}$). Even at high pump powers, about 10% of Pr³⁺ ions in highly doped PDFs stay in the ground state. Pumping efficiency is lost due to a fast up-conversion that occurs when both ions in a pair are pumped.

By varying the length of the praseodymium doped fiber at various pump strength, one can perceive the progression of the gain of the PDFA when the concentration of Pr³⁺ ions is $50 \times 10^{24} \text{ ions m}^{-3}$, as shown in Fig. 5a. It is clear that when the 5 m PDF and 100 mW pump power are used, the PDFA's maximum gain is about 1 dB. The trend of decreasing gain increases with PDF length and is caused by a decline in population inversion. Thus, 5 m is found to be the optimal length for the PDF that produces the highest gain. Gain versus input signal power plots for various Pr³⁺ ion concentrations are displayed.

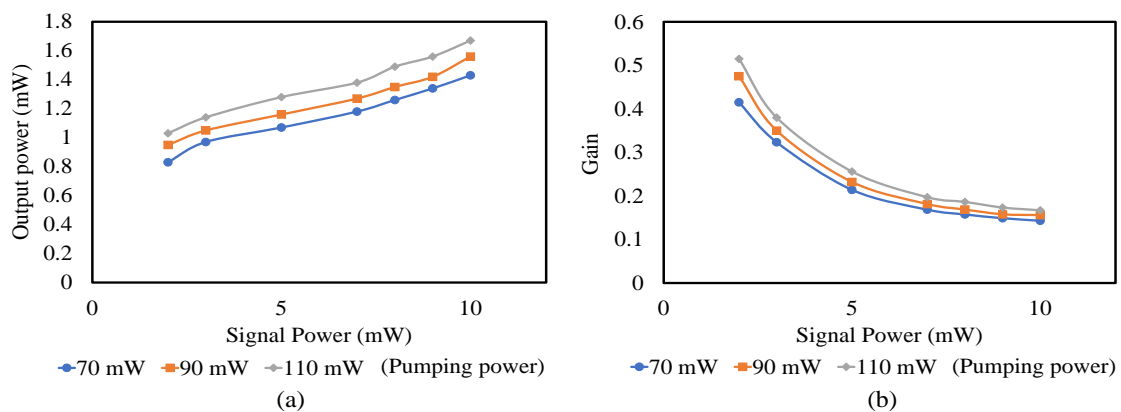


Figure 5: (a) Signal power vs. Output power (b) Signal power vs. gain at different pump power

To estimate the PCE of the PDFA, draw pump control against output control as a province of input signal energy for a given PDF length. Figure 6a illustrates that the PCE value reaches its maximum of 4% at 8.8 dBm of input signal power and its minimum of 2% at 2.3 dBm of input signal power. Scheming the pump wavelength contrary to the output strength of the input signal allows to examine how a change in the pump wavelength affects the output power of the amplifier.

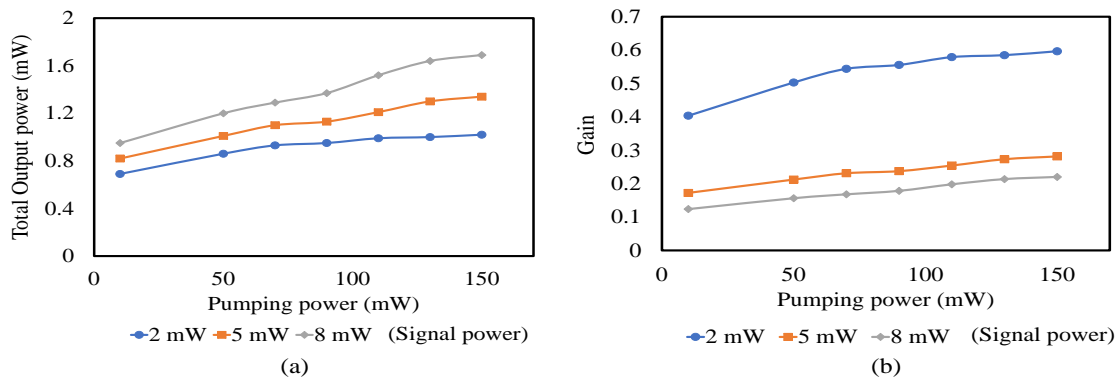


Figure 6: (a) Pumping power vs. Output power (b) Pumping power vs. gain at different signal power

CONCLUSION

Opti_System simulation files are used to evaluate the praseodymium doped fiber amplifier's performance and visualization. The findings indicate that an optimized praseodymium doped fiber length of roughly 5 m can achieve a peak gain of about 1 dB for an maximized pumped power of 300 mW, and input signal wavelength of 635 nm. This discovery has important implications for all visible fiber ultrasort pulsed lasers.

Declaration by Authors

Acknowledgement: None

Source of Funding: None

Conflict of Interest: The authors declare no conflict of interest.

REFERENCES

1. Y. Dogan and K. Madsen, (2020) "Optimization of ultrafast laser parameters for 3D micromachining of fused silica," *J. Optics and Laser Technology*, Vol. 123, No. 105933.
2. T. Chen, R. Fardel and C. B. Arnold, (2018) "Ultrafast z-scanning for high efficiency lase micro-machining," *J. Light: Science and Application*, Vol. 7 pp. 17181.
3. T. Fortier and E. Baumann, (2019) "20 years developmens in optica frequency comb technology and applications", *J. Communication Physics*, Vol. 2, No. 153.
4. V. Duran, S. Tainta, and V. Torres-company, (2015) "Ultrafast electroptic dual-comb interferometry," *J. Optics and Laser Technology*, Vol. 23, No. 23.
5. Mark D. Mackenzie et al., (2019) "GLS and GLSSe ultrafast laser inscribed waveguides for mid-IR supercontinuum generation," *J. Optical Materials Express*, Vol. 9, No. 2.
6. L. G. Zhu et al., (2009) "Ultrafast phenomena and terahertz waves: introduction," *J. Optical Society of America B*, Vol. 39, No. 3, pp. 1–17.
7. B. Cao et al., (2023) "Spatiotemporal mode-locking and dissipative solitons in multimode fiber lasers," *J. Light: Science and Application*, Vol. 12, No. 260.
8. C. Jiang and L. Jin, (2009) "Numerical model of an Er³⁺-Tm³⁺-Pr³⁺- codoped fiber amplifier pumped with an 800 nm laser diode," *J. Applied Optics*, Vol. 48, No. 12.

9. Arlee V. Smith and Jesse J. Smith., (2013) "Increasing mode instability thresholds of fiber amplifiers by gain saturation," *J. Optics Express*, Vol. 21, No. 13 January, pp. 15168-15182.
10. P. Chen et al., (2012) "Crystal Fiber Based Erbium Doped Amplifiers and Their Gain," *J. Future Computer and Communication*, Vol. 1, No. 1.
11. N. Boetti et. al., (2022) "High concentration Er-doped phosphate glass optical fibers for single-frequency fiber amplifiers," *SPIE Proceedings*, Vol. PC12140.
12. C. C. Baker et. al., (2019) "Rare earth co-doping for increased efficiency of resonantly pumped Er-fiber lasers," *J. Optical Material Express*, Vol. 9, No. 3.
13. P. Xing et al., (2017) "Silicon rich nitride ring resonators for rare – earth doped telecommunications-band amplifiers pumped at the O-band," *Scientific Reports*, Vol. 7, No. 9101.
14. N. Yu et. al., (2022) "Optically Managing Thermal Energy in High-power Yb-doped Fiber Lasers and Amplifiers: A Brief Review," *Current optics and Photonics*, Vol. 6, No. 6, pp. 521–549.
15. J. M. Knall et al., (2021) "Radiation-Balanced Silica Fiber Amplifier," *J. Physics Review Letter*, Vol. 121, No. 013903.
16. M. H. Yuan et al., (2015) "Upconversion luminescence from aluminoborate glasses doped with Tb³⁺, Eu³⁺ and Dy³⁺ under the excitation of 2.6- μ m femtosecond laser pulses," *J. Optics Express*, Vol. 23, No. 17.
17. O. Henderson-Sapir et al., (2017) "Recent Advances in 3.5 μ m Erbium-Doped Mid-Infrared Fiber Lasers," *IEEE Journal of Selected Topics in Quantum Electronics*, Vol. 23, No. 3, pp. 1–9.
18. T. san et. al., (2021) "Progress and Summary of Photodarkening in Rare Earth Doped Fiber," *J. Applied Science*, Vol. 11, No. 21.
19. M.Z. Amin, K.K. Qureshi, and M.M.Hossain, (2019) "Doping radius effects on an erbium-doped fiber amplifier," *J. Chin. Opt. Lett.* vol. 17, no.1, 010602.
20. C. Jiang, (2009) "Modeling and gain properties of er³⁺ and pr³⁺ codoped fiber amplifier for 1.3 and 1.5 μ m windows," *J. OSA B*, Vol. 26, No. 5, pp. 1049–1056.
21. S. Mukhtar, K.N. Aliyu, K. Qureshi, (2020) "Performance evaluation of er³⁺/yb³⁺ codoped fiber amplifier," *J. Microw. Opt. Technol. Lett.* Vol. 62, No. 6, pp. 2243–2247.
22. M.C. aul et. at., (2015) "Enhanced erbiumzirconia-yttria-aluminum co-doped fiber amplifier," *J. IEEE Photonics* Vol. 7, No. 5, pp. 1–7.
23. L. Shen, B. Chen, H. Lin, and E. Pun, (2015) "Praseodymium ion doped phosphate glasses for integrated broadband ion-exchanged waveguide amplifier," *J. Alloys Compd.*, Vol. 622, pp. 1093–1097.
24. L. horchos and J. P. Turkiewicz, (2017) "Experimental performance of semiconductor optical amplifiers and praseodymium-doped fiber amplifiers in 1310-nm dense wavelength division multiplexing system," *J. Opt. Eng.* Vol. 56, No. 4, 046101.
25. E.A. Anashkina, A.V. Kim, (2017) "Numerical simulation of ultrashort mid-ir pulse amplification in praseodymium-doped chalcogenide fibers," *J. Lightwave Technol.* Vol. 35, No.24, pp. 5397–5403.
26. M. Shen et. al., (2018) "Modeling of resonantly pumped mid-infrared pr³⁺-doped chalcogenide fiber amplifier with diferent pumping schemes," *J. Opt. Express* Vol. 26, No. 18, pp. 23641–23660.
27. Opti system, (2021) "optisystem overview.: <https://www.optiwave.com/optisystem-overview/>".
28. A. J. Steck et. al., (2007) " Prospects for rare earth doped GaN lasers on Si," *J. Materials Today*, Vol. 10, No. 7,8, pp. 20-27.
29. J. Mirza et. al., (2011) "Performance evaluation of praseodymium doped fiber amplifiers," *Optical Review*.

How to cite this article: Nasrin Sultana, Md. Abubakar Siddik. Characterization of visible range gain in praseodymium doped fiber amplifier. *International Journal of Research and Review*. 2024; 11(1): 140-146. DOI: <https://doi.org/10.52403/ijrr.20240115>
